Smectic-A_1-to-nematic phase transition: X-ray diffraction of the bulk and comparison with surface structure

E. F. Gramsbergen*
Solid State Physics Laboratory, Melkweg 1, NL-9718 EP Groningen, The Netherlands

J. Als-Nielsen
Risø National Laboratory, DK-4000 Roskilde, Denmark

W. H. de Jeu†
FOM Institute for Atomic and Molecular Physics, Foundation for Fundamental Research on Matter, Kruislaan 407, NL-1098 SJ Amsterdam, The Netherlands

(Received 22 June 1987)

We report x-ray scattering measurements around the smectic-A_1-to-nematic phase transition of $C_8H_{17}O$-ϕ-OOC-ϕ-OCH_2-ϕ-CN, where ϕ is the phenylene functional group. Critical fluctuations occur at the smectic-A_1 monolayer wave vector $\mathbf{q}_2$ and noncritical bilayer fluctuations at the incommensurate wave vector $\mathbf{q}_1 \approx 0.56\mathbf{q}_2$. This is different from the situation at the surface where the two wave vectors are commensurate with $\mathbf{q}_1 = \frac{1}{2}\mathbf{q}_2$. For both types of layering the correlation lengths for the bulk were found to be equal to the penetration depths at the surface. The critical behavior of the monolayer fluctuations is described by the critical exponents γ for the susceptibility and $\nu_\parallel$ for the correlation length, which are both close to their tricritical values. This is unexpected for the large nematic temperature range involved.

I. INTRODUCTION

In smectic-A (S_A) liquid crystals rod-shaped molecules are orientationally ordered and segregated into stacks of two-dimensional layers. The first observation of a phase transition between two smectic-A phases[1] triggered the discovery of S_A polymorphism in many systems where strongly asymmetric molecules with large terminal dipoles are involved.[2] Phase diagrams show at least four different S_A phases. The x-ray patterns of nematic and these particular S_A phases are shown in Fig. 1. A common feature of all these phases is the presence of two competing density waves. Their wave vectors $\mathbf{q}_1$ and $\mathbf{q}_2$ may be either commensurate with $\mathbf{q}_1 = \frac{1}{2}\mathbf{q}_2$, or incommensurate with $\frac{1}{2}q_2 < q_1 < q_2$. In all these cases, q_2 is approximately equal to $2\pi/l$, where l is the molecular length. The scattering around $\mathbf{q}_1$ is associated with the dipolar ordering of the molecules, which favors antiparallel coupling of the polar heads. The most common among these phases is the S_{Ad} phase. It has a Bragg[3] peak at $\mathbf{q}_1$ and diffuse scattering at $\mathbf{q}_2$, with $\frac{1}{2}q_2 < q_1 < q_2$. On the microscopic level, it can be understood as a layering of molecules lying head to head with a partial overlap (dimers), thus forming layers with thickness between one and two molecular lengths.

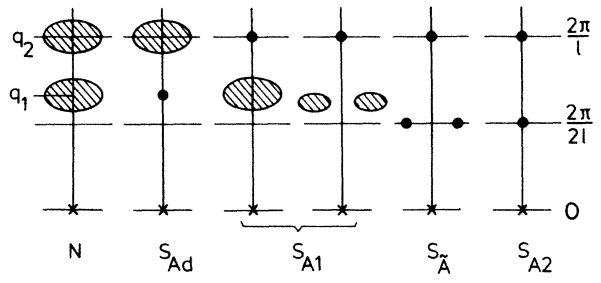

FIG. 1. X-ray diffraction patterns of nematic (N) and smectic-A (S_A) phases with strongly polar molecules. The vertical axis is along the director $\hat{\mathbf{n}}$ in the $q_\parallel$ direction and the horizontal axis in the $q_\perp$ plane, which is parallel to the smectic layers. Crosses denote the direct beam, solid points are Bragg reflections, and hatched areas are diffuse scattering. The monolayer ordering ($d = l$) produces the scattering at $\mathbf{q}_2$ and the dipolar ordering ($l < d \leq 2l$) produces the scattering at $\mathbf{q}_1$.

In the S_{A_2} phase, both density waves are (quasi) long range, as inferred from the presence of two Bragg peaks, and $\mathbf{q}_1$ locks in at $\frac{1}{2}\mathbf{q}_2$. This is interpreted as an antiferroelectric layer structure with the dipolar orientation alternating from layer to layer. In the S_{A_1} phase, there is a Bragg spot at $\mathbf{q}_2$ and a diffuse spot at $\mathbf{q}_1$ with q_1/q_2 varying from 0.5 to 0.7. At lower temperatures, this spot may be split into two diffuse spots off-axis ($q_{\perp 1} \neq 0$), corresponding to a modulation in the direction of the layers. In addition, an $S_{\tilde{A}}$ phase[4] is observed where this modulation is long range. Since recently, an incommensurate smectic-A phase ($S_{A\mathrm{ic}}$) is known with two collinear density waves that are both long range,[5] it is not clear how this phase should be interpreted microscopically. All S_A phases are successfully described, however, in a unified picture by a phenomenological model incorporating two complex order parameters for the two density waves, and a free energy with elastic terms

favoring incommensurability and a coupling term favoring commensurability.[6] Competition between these two terms leads to frustration and the system responds by the formation of various S_A phases.

In this paper we adhere to the interpretation of the S_{A_1} phase on a molecular level. X-ray reflectivity measurements of the surface of an S_{A_1} liquid crystal showed the development of a few antiferroelectric S_{A_2}-like bilayers at the interface.[7] This surface effect could be the result of an antiferroelectric short-range order already present in the bulk. In order to answer this question, we measured the bulk correlation lengths for the monolayering and bilayering of the same material around the S_{A_1}-N phase transition. They were both found to be equal to the corresponding penetration depths at the surface. The result for the bilayers is new and suggests for the bulk an interpretation of the S_{A_1} phase as *disturbed* S_{A_2}.[8,9] In addition, the critical behavior of the monolayer fluctations is considered. The critical exponents γ for the susceptibility and $\nu_{\|}$ for the correlation length are both close to their tricritical values. This is unexpected for the large nematic temperature range involved.

II. EXPERIMENT

The x-ray scattering experiments were carried out with two different configurations of the spectrometer. A low-resolution configuration with a position-sensitive detector (PSD) was used to study the short-range bilayering near q_1. Higher resolution was required to study the condensation of the monolayer peak at q_2. A high-resolution triple axis configuration (TAS) was used for this purpose, at the cost of x-ray intensity.

The high-resolution triple axis setup is shown in Fig. 2(a). The x-ray source (A) is a Rigaku copper rotating anode operated at 50 kV and 180 mA with a focal spot height of 1 mm and width 10 mm, the latter being reduced to 1 mm effectively by the viewing angle of approximately 6°. Together with the monochromator slit (B) of width 2 mm at 400 mm from the source, this produces a beam with an angular collimation of 0.5°. A (1,1,1) reflection on a properly aligned ($\Theta_B = 14.2°$) Si monochromator crystal (C) reflects the $K\alpha_1$ and $K\alpha_2$ wavelengths. The Darwin width determined angular divergence of each component is 0.004° FWHM; their mutual separation is 0.036° in the horizontal plane. This allows for elimination of the $K\alpha_2$ component by the monochromator output slit (D), 1-mm wide at 300 mm from the monochromator. This slit also reduces the continuous (Bremsstrahlung) background. The sample oven is mounted on one of the two turntables of a double goniometer (E), placed 335 mm behind the monochromator and centered on the $K\alpha_1$ beam. The second circle holds the analyzer arm, with the analyzer input slits (F) and a Si analyzer crystal (C') similar to the monochromator, at 335 and 380 mm, respectively, behind the sample, and a NaI scintillation counter (G) to detect the scattered x-ray photons. The rotation angles of the sample and the analyzer arm are denoted as ω and 2Θ, respectively. The vertical extent of the beam incident on the monochromator, sample, and analyzer is determined by additional slits in the vertical plane at B, D, and F with approximate heights of 4, 2, and 2 mm, respectively. Evacuated tubes with kapton windows between the monochromator and slit D, and between the sample oven and slit F, reduce absorption and scattering in the air, gaining a factor 1.5 in intensity.

With the monochromator and analyzer crystals set to reflect in opposite directions, the spectrometer is in the nondispersive mode, so the natural linewidth of the $K\alpha_1$ line has no influence on the resolution. The experimentally found resolution is roughly 0.006° FWHM (2Θ), which is in the order of magnitude of the Darwin width of the crystals. In reciprocal space, this amounts to 4×10^{-4} Å^{-1} along q_z [see Fig. 2(c)]. The resolution in the vertical direction (q_y), determined by the vertical slits at D and F, is approximately 0.02 Å^{-1} (FWHM).

The low-resolution configuration is shown in Fig. 2(b). The monochromator (C) is a single-bent graphite crystal curved in the vertical plane with a radius of 1100 mm for collimation on the PSD (G). The slits D and D', located 77 and 300 mm from the monochromator and 0.13-mm wide each, define the beam incident on the sample with an angular collimation of 0.034° FWHM. The PSD, with a 45-mm long detector wire and placed asymmetrically at 630 mm from the sample, collects the scattered photons. A beam stop placed 120 mm behind

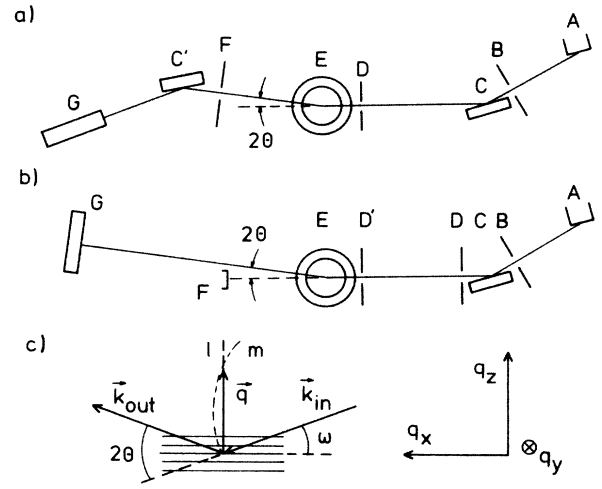

FIG. 2. Schematic diagram of the two configurations of the x-ray scattering apparatus shown in the horizontal plane. (a) High-resolution triple axis setup, with A, rotating anode x-ray generator; B, monochromator input slits; C,C', Si (111) monochromator and analyzer crystals; D, monochromator output slits; E, two-circle sample table; F, analyzer input slits; G, NaI scintillation detector. (b) Low-resolution setup, with A, B, and E as in (a); C, single-bent graphite monochromator crystal; D,D', beam-defining slits; F, direct beam stop; G, position sensitive detector (PSD). (c) The sample with the smectic layers, the angles ω and 2Θ, and the laboratory fixed set of axes q_x,q_y,q_z in reciprocal space. In a $(\Theta,2\Theta)$ scan, $\omega=\Theta$ and the scan is along the straight line l in reciprocal space. When using the PSD, ω is constant and the scan is along the circle m, which is part of the Ewald sphere. The director orientation is determined by the magnetic field (0.4 T) provided by permanent magnets.

the sample prevents the beam from hitting the PSD. The signal from the PSD is fed into a 1200-channel multichannel analyzer (MCA), providing a detector resolution of 0.039 mm or 0.004° (2Θ) per channel. The overall resolution, which is dominated by the width of slits D and D', is approximately 0.05° (2Θ) or 4×10^{-3} Å^{-1} (FWHM) along q_z in reciprocal space. Without the presence of additional vertical slits, the resolution in q_y is determined by the illuminated sample height of 6 mm to be approximately 0.04 Å^{-1} (FWHM). The $\Delta\lambda/\lambda$ contribution from the presence of both $K\alpha$ lines is negligible for the small scattering angles used in the experiment.

The liquid crystal is held in a sample holder with Be widows; the cell thickness is approximately 2 mm and lateral dimensions are 13 mm×13 mm. The cell is placed in a two-stage oven. The outer stage is heated to a few degrees below the temperature of the inner stage, which is electronically controlled with a stabilization better than 0.03 °C. Built-in permanent magnets provide a field of 0.4 T for alignment of the director in the sample.

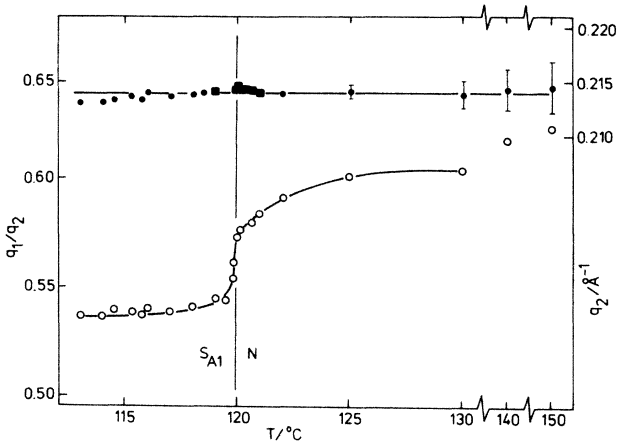

FIG. 3. The monolayer wave number q_2 (scale right), measured with PSD (solid circles) and TAS (squares), and the ratio q_1/q_2 (open circles, scale left), measured with PSD vs temperature, in the S_{A_1} and N phases. The lines are guides for the eye. The horizontal line is at the level 0.214 Å^{-1}.

III. RESULTS

The compound studied is (with ϕ being the phenylene functional group)

$$C_8H_{17}O-\phi-OOC-\phi-OCH_2-\phi-CN\ ,$$

which has the following sequence of phase transitions[10] (K stands for crystalline, $S_{\tilde{C}}$ for the tilted analogue of $S_{\tilde{A}}$, I for isotropic liquid):

$$K \overset{112\,^\circ C}{\leftrightarrow} S_{\tilde{C}} \overset{113\,^\circ C}{\leftrightarrow} S_{A_1} \overset{120\,^\circ C}{\leftrightarrow} N \overset{166\,^\circ C}{\leftrightarrow} I\ .$$

The S_{A_1}-N transition temperature T_{AN} in the sample was determined from the condensation of the monolayer reflection in the TAS setup, by inspection of both linewidth and intensity. By making a few quick scans (typically 1 min) while the temperature was slowly drifting we could locate $T_{AN}=119.92\pm0.02$ °C. The drift in T_{AN} due to sample degradation was roughly 0.1 °C in 24 h and the mosaic spread in the sample was typically 1°. As a consequence of the broad vertical resolution in either configuration of the spectrometer, the detector integrates over this mosaic spread in the vertical direction (*not* in the horizontal direction).

Above the S_{A_1}-N phase transition, the scattering shows two diffuse incommensurate peaks at $\mathbf{q}_1$ and $\mathbf{q}_2$; at the transition towards the S_{A_1} phase the peak at $\mathbf{q}_2$ condenses. The evolution of the two peaks was followed over a large temperature range using the PSD. The temperature dependence of q_2 and q_1/q_2 is displayed in Fig. 3. The value of q_2 is remarkably constant and close to $2\pi/l$, with the molecular length $l=29.8$ Å as obtained from a space-filling model. At low temperature the ratio q_1/q_2 is nearly constant at the value 0.54. When going up in temperature, q_1/q_2 increases further away from the commensurate value of $\frac{1}{2}$, with quite a drastic change at the S_{A_1}-N phase transition. Inspection of x-ray photographs show that, in addition, the diffuse peak at $\mathbf{q}_1$ splits into two peaks off-axis at temperatures below approximately 117 °C.

The intensities of the two peaks, integrated over q_z, are shown in Fig. 4. A few degrees above T_{AN} the condensation of the monolayer peak is preempted by a strong increase in intensity, as may be expected for a second-order phase transition. The increase is more pronounced in the TAS than in the PSD measurements, due to the different vertical resolutions of the two methods: when the transverse correlation length exceeds the resolution width, the two methods collect different fractions of the total scattering along q_y. Gradual changes in the mosaicity profile in the horizontal plane, which might in

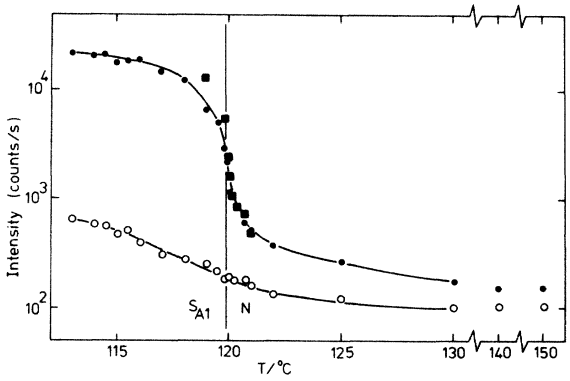

FIG. 4. The integrated intensities of the reflections at $\mathbf{q}_1$ and $\mathbf{q}_2$ vs temperature in the S_{A_1} and N phases. The logarithmic intensity scale is for the PSD measurements integrated over the PSD channels; for the TAS data, which are integrated over q_z, an arbitrary scaling factor has been adopted. Open (closed) symbols refer to bilayer (monolayer) fluctuations; circles (squares) refer to PSD (TAS) measurements. The lines are guides for the eye.

principle affect the intensity detected by the PSD, are negligible in practice. In the TAS setup, no change in mosaicity was observed once the smectic layers were established.

The longitudinal correlation lengths of the fluctuations at $\mathbf{q}_1$ and $\mathbf{q}_2$ were calculated by fitting the measured intensity profiles with a Lorentzian convoluted with the resolution function of the TAS or PSD setup. The actual convolution was performed using an approximated trapezoidal shape for the resolution function; this results in a relatively easy analytical expression for the intensity profile. In this calculation subtle effects due to the limited vertical resolution[11] were neglected; the implications of this will be discussed below. The results are shown in Fig. 5. Far from T_{AN} in the nematic phase, the monolayer and bilayer correlation lengths are roughly equal and of molecular dimensions. The monolayer correlation length $\xi_{\parallel 2}$ diverges towards T_{AN} to become long range in the smectic phase; the bilayer correlation length $\xi_{\parallel 1}$ develops continuously through the S_{A_1}-N phase transition. In the smectic phase itself, however, there is a strong increase in $\xi_{\parallel 1}$ with decreasing temperature. Below 117 °C the data become less reliable because the bilayer peak splits into two peaks off the $q_\parallel$ axis.

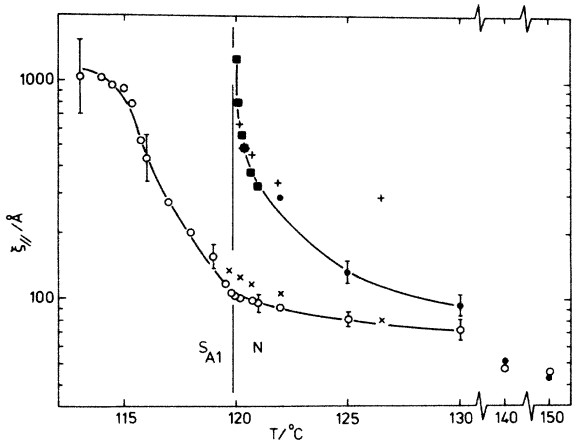

FIG. 5. The correlation length $\xi_{\parallel 1}$ of the bilayering, measured with the PSD (open circles), and $\xi_{\parallel 2}$ of the monolayers, measured with PSD (closed circles) and TAS (squares). The crosses give the monolayer (+) and bilayer (×) penetration depths at the surface (from Ref. 7). The lines are guides for the eye.

IV. DISCUSSION

One of the objectives of the present research was to compare the bulk and surface structure of the S_{A_1} phase. We therefore first summarize the conclusions reached from the measurement of surface x-ray reflectivity on both sides of the S_{A_1}-N phase transition.[7] (1) At the surface, monolayers develop with a penetration depth $\xi_{\parallel 2}$ into the bulk that diverges as the smectic phase is approached. (2) In addition, a few bilayers develop due to the dipolar ordering within the layers. Inherent to the molecular model that was developed to account for the observed reflectivity curve, the monolayering and bilayering are commensurate with $\mathbf{q}_1 = \frac{1}{2}\mathbf{q}_2$. (3) The monolayering and bilayering are both saturated at the surface, i.e., there is a fully developed top layer that is completely polarized. (4) The decay of the bilayering into the bulk cannot be described with a simple exponential. It decays more abruptly and is well described with an S-shaped curve with a characteristic length $\xi_{\parallel 1}$ and an additional shape parameter J.

The values of $\xi_{\parallel 1}$ and $\xi_{\parallel 2}$ are given in Fig. 5. For $\xi_{\parallel_1}$ as well as $\xi_{\parallel 2}$, the values for surface and bulk are approximately equal. (The point at 126 °C of $\xi_{\parallel 2}$ for the surface is based on a very small signal and much less accurate.) The behavior of $\xi_{\parallel 2}$ is similar to earlier findings, where near nematic to S_{Ad} (Refs. 12-14) and S_{A_1} (Ref. 15) phase transitions bulk and surface correlation lengths of the diverging density wave were found to be equal. As for the bilayers, the equality of the surface and bulk values of $\xi_{\parallel 1}$ is new and requires some more comment. For the surface, $\xi_{\parallel 1}$ is the characteristic length of a nonexponential decay, while the bulk value is related to an exponential correlation function; yet they are equal. A similar case of equal characteristic lengths for nonexponential behavior at the surface and an exponential correlation function in the bulk is the well-known liquid-vapor interface.[16] Another possibility is that the correlations in the bulk do not behave exponentially either. This would in principle lead to a deviation from the Lorentzian line shape which is, however, not detectable with our PSD resolution and signal-to-background ratio. The very fact that deviations of this kind were so clearly detectable at the surface lies in the destructive interference of the layering and Fresnel signals in certain $\mathbf{q}$ regions, so that small deviations in one of these signals lead to large relative changes in the reflectivity.

Very remarkable with respect to the comparison between bulk and surface is that at the surface the bilayer wave vector $\mathbf{q}_1$ locks in at $\frac{1}{2}\mathbf{q}_2$, whereas in the bulk these wave vectors are incommensurate with q_1/q_2 varying from 0.54 to 0.60 in the temperature range that was covered by the surface measurements. This is contrary to the behavior of the compound DB_7NO_2, where bulk and surface are both incommensurate with the same wave vectors $\mathbf{q}_1$ and $\mathbf{q}_2$.[15] In the latter case, the data were fit with two density waves with arbitrary amplitude and phase at the surface. In order to find out weather the difference with our case is real or just an artifact of the model, we tried to fit the surface data in Ref. 7 in a similar way with q_1/q_2 fixed to the bulk values. This did not result in satisfactory fits, so that the difference must be real. What this means on a molecular level is not very clear, because the model used for DB_7NO_2 lacks a clear molecular interpretation. An additional difference lies in the relation between surface and bulk values of $\xi_{\parallel 1}$: as pointed out above, we find equal values for surface and bulk, whereas in DB_7NO_2 they are different.

We cannot exclude the possibility that models which differ from ours in certain respects produce equally good

fits to the reflectivity data. One possibility, for example, is that the molecules at the surface are tilted through dielectric forces induced by a gradient of the orientational order parameter.[17] Although more detailed information is required to judge about such subtle modifications to our model, the general picture of the surface as developed in Ref. 7 has to be maintained. As this surface is in fact S_{A_2}-like, the equality of $\xi_{\parallel 1}$ for surface and bulk then suggests an interpretation of the S_{A_1} phase as locally S_{A_2}, with irregularly spaced shifts of the bilayer density wave over one molecular length.[8,9,18] It differs from the $S_{\tilde{A}}$ phase in that these shifts are not regularly spaced. The strong antiferroelectric short-range order that naturally follows from such a model is supported by dielectric measurements.[19]

We finally consider the critical behavior of the diverging monolayer fluctuations just above the second-order S_{A_1}-N phase transition. The intensity of scattering is commonly described with the modified Ornstein-Zernike expression[11,12,20–22]

$$S(\mathbf{q})=\frac{\sigma}{1+\xi_{\parallel 2}^2(q_\parallel-q_2)^2+\xi_{\perp 2}^2 q_\perp^2+c\xi_{\perp 2}^4 q_\perp^4}\ .$$

The critical behavior is contained in the susceptibility σ and the correlation lengths $\xi_{\parallel 2}$ and $\xi_{\perp 2}$; the fourth-order term $c\xi_{\perp_2}^4 q_\perp^4$ is phenomenological without a clear theoretical justification. The values of σ and $\xi_{\parallel 2}$ obtained by deconvoluting $q_\parallel$ scans with the longitudinal resolution function are displayed as a function of $t=(T-T_{AN})/T_{AN}$ in Fig. 6. In should be realized that $\xi_{\parallel 2}$, $\xi_{\perp 2}$, σ, and c become coupled in a complicated way when the transverse correlation length $\xi_{\perp 2}$ becomes comparable to the inverse of the transverse resolution width. An estimate of $\xi_{\perp 2}$ is obtained by taking an ω scan (rocking curve) of the sample, which is approximately equivalent to a $q_\perp$ scan, through the middle of the monolayer peak. It is found that $\xi_{\perp 2}$ is a factor 5 to 10 lower than $\xi_{\parallel 2}$. With the vertical resolution of the PSD of 0.02 Å^{-1} FWHM, this makes $\xi_{\parallel 2}$ and σ effectively decoupled from $\xi_{\perp 2}$ and c when $t>0.5\times 10^{-3}$. Points closer to the S_{A_1}-N phase transition receive and extra uncertainty in the order of 15% for $\xi_{\parallel 2}$ and 30% for σ (both at $t=0.3\times 10^{-3}$). The behavior of $\xi_{\parallel 2}$ and σ in the temperature range covered by the PSD measurements is well described by the critical exponents $\nu_\parallel=0.52\pm 0.06$ and $\gamma=1.06\pm 0.10$, respectively, where the error bounds arise largely from the uncertainty of the critical temperature (± 0.02 °C). One should be aware that these exponents are established over only one decade in t, which is not enough to exclude the possibility of some kind of crossover behavior. Nevertheless, it is remarkable that the measured exponents are close to the mean-field tricritical values $\nu_\parallel=0.5$ and $\gamma=1$, while the McMillan ratio[23] $T_{AN}/T_{NI}=0.895$ is small compared to the value of about 0.98–0.99 usually found for the S_A-N tricritical point. For McMillan ratios in this range, the exponents usually tend to higher values like $\nu_\parallel=0.8$ and $\gamma=1.5$.[12,20–22] The number of exceptions, however, seems to be steadily growing. In the compounds T7 and T8, with an extremely small McMillan ratio of approximately 0.7, the trend reverses and S_{A_1}-N exponents are close to the XY values $\nu_\parallel=0.67$ and $\gamma=1.32$ (Ref. 24) as originally predicted for the S_A-N transition.[25] In the DB_6-TBBA system, S_{A_1}-N critical exponents cross over to nearly tricritical values on approaching the N-S_{A_1}-S_{A_2} triple point.[11] Most surprising of all is a mixture (CCH_4-1A9F) where a first-order S_{A_1}-N phase transition with large latent heat, above an $S_{\tilde{A}}$-S_{A_1} transition, occurs with a McMillan ratio of 0.93.[26] In DB_6-TBBA, the S_{A_1}-N critical behavior is probably influenced by coupling of the smectic-order parameter to an additional order parameter of the S_{A_2} phase, while in CCH_4-1A9F local structural changes by complex formation are responsible for the anomalous behavior. In our case, the coupling to $S_{\tilde{C}}$ order parameters may play a role; in the S_{A_1} phase itself this coupling is evidenced by the splitting off-axis of the scattering near $\mathbf{q}_1$.

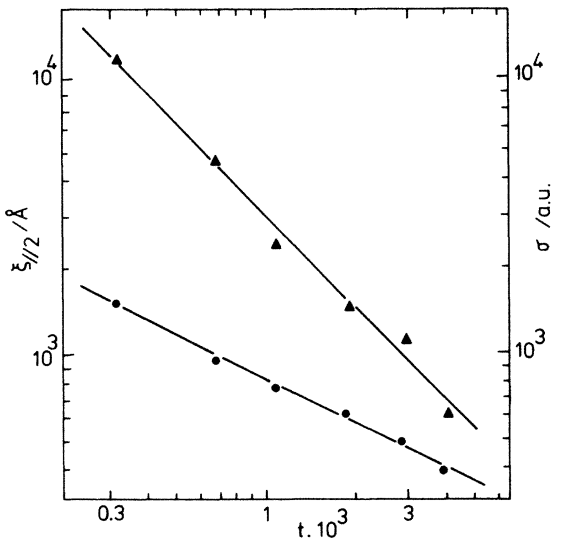

FIG. 6. The monolayer correlation length $\xi_{\parallel 2}$ (circles) and the susceptibility σ (triangles) vs reduced temperature $t=(T-T_{AN})/T_{AN}$. The lines correspond to the critical exponents $\nu_\parallel=0.52$ and $\gamma=1.06$, respectively.

ACKNOWLEDGMENT

The authors wish to thank Professor G. Heppke (Technische Universität Berlin) for providing them with the substance. The excellent research conditions provided by the Risø National Laboratory (Roskilde, Denmark) are gratefully acknowledged. This work forms part of the research program of the Stichting voor Fundamenteel Onderzoek der Materie (Foundation for Fundamental Research on Matter, FOM) and was made possible by financial support from the Nederlandse Organisatie voor Zuiver Wetenschappelijk Onderzoek (Netherlands Organization for the Advancement of Pure Research, ZWO).

*Present address: Laboratory for Physical Chemistry, University of Amsterdam, Nieuwe Achtergracht 127, NL-1018 WS Amsterdam, The Netherlands.

†Also at The Open University, Postbox 2960, NL-6401 DL Heerlen, The Netherlands.

[1](a) G. Sigaud, F. Hardouin, and M. F. Achard, Phys. Lett. **72A**, 24 (1979); (b) G. Sigaud, F. Hardouin, M. F. Achard, and H. Gasparoux, J. Phys. (Paris) Colloq. **40**, C3-356 (1979).

[2]For a review, see F. Hardouin, A. M. Levelut, M. F. Achard, and G. Sigaud, J. Chim. Phys. **80**, 53 (1983).

[3]Strictly speaking, there is only *quasi*-long-range order in S_A phases: J. Als-Nielsen, J. D. Litster, R. J. Birgeneau, M. Kaplan, C. R. Safinya, A. Lindegaard-Andersen, and S. Mathiesen, Phys. Rev. B **22**, 312 (1980).

[4]In fact, two types of $S_{\tilde{A}}$ phase can be distinguished: A. M. Levelut, J. Phys. (Paris) Lett. **45**, L-603 (1984).

[5]B. R. Ratna, R. Shashidhar, and V. N. Raja, Phys. Rev. Lett. **55**, 1476 (1985).

[6](a) J. Prost and P. Barois, J. Chim. Phys. **80**, 65 (1983); (b) P. Barois, J. Prost, and T. C. Lubensky, J. Phys. (Paris) **46**, 391 (1985).

[7]E. F. Gramsbergen, W. H. de Jeu, and J. Als-Nielsen, J. Phys. (Paris) **47**, 711 (1986).

[8]L. Longa and W. H. de Jeu, Phys. Rev. A **28**, 2380 (1983).

[9]W. H. de Jeu, *Structural Incommensurability in Crystals, Liquid Crystals and Quasi-Crystals,* Vol. 166 of *NATO Advanced Study Institute Series,* edited by J. F. Scott (Plenum, New York, 1987).

[10](a) Nguyen Huu Tinh and C. Destrade, Mol. Cryst. Liq. Cryst. **92**, 257 (1984); (b) F. Hardouin, M. Achard, C. Destrade, and Nguyen Huu Tinh, J. Phys. (Paris) **45**, 765 (1984).

[11]K. K. Chan, P. S. Pershan, and L. B. Sorensen, Phys. Rev. A **34**, 1420 (1986).

[12]P. S. Pershan, A. Braslau, A. H. Weiss, and J. Als-Nielsen, Phys. Rev. A **35**, 4800 (1987).

[13]J. Als-Nielsen, F. Christensen, and P. S. Pershan, Phys. Rev. Lett. **48**, 1107 (1982).

[14]P. S. Pershan and J. Als-Nielsen, Phys. Rev. Lett. **52**, 759 (1984).

[15]B. M. Ocko, P. S. Pershan, C. R. Safinya, and L. Y. Chiang, Phys. Rev. A **35**, 1868 (1987).

[16]See, for example, (a) B. Widom, in *Phase Transitions and Critical Phenomena,* edited by C. Domb and M. S. Green (Academic New York, 1972), Vol. 2; (b) J. S. Rowlinson and B. Widom, *Molecular Theory of Capillarity* (Clarendon, Oxford, 1982).

[17]G. Barbero, I. Dozov, J. F. Palierne, and G. Durand, Phys. Rev. Lett. **56**, 2056 (1986).

[18]E. F. Gramsbergen and W. H. de Jeu, J. Phys. (Paris) **49** (1988).

[19](a) L. Benguigui and F. Hardouin, J. Phys. (Paris) Lett. **42**, L-381 (1981); (b) L. Benguigui, F. Hardouin, and G. Sigaud, Mol. Cryst. Liq. Cryst. **116**, 35 (1984).

[20](a) R. J. Birgeneau, C. W. Garland, G. B. Kasting, and B. M. Ocko, Phys. Rev. A **24**, 2624 (1981); (b) C. W. Garland, M. Meichle, B. M. Ocko, A. R. Kortran, C. R. Safinya, L. J. Yu, J. D. Litster, and R. J. Birgeneau, *ibid.* **27**, 3234 (1983).

[21]A. R. Kortran, H. von Känel, R. J. Birgeneau, and J. D. Litster, J. Phys. (Paris) **45**, 529 (1984).

[22](a) B. M. Ocko, R. J. Birgeneau, J. D. Litster, and M. E. Neubert, Phys. Rev. Lett. **52**, 208 (1984); (b) B. M. Ocko, R. J. Birgeneau, and J. D. Litster, Z. Phys. B **62**, 487 (1986).

[23]W. L. McMillan, Phys. Rev. A **4**, 1238 (1971).

[24]K. W. Evans-Lutterodt, J. W. Chung, B. M. Ocko, R. J. Birgeneau, C. Chiang, C. W. Garland, J. Goodby, and Nguyen Huu Tinh, Phys. Rev. A **36**, 1387 (1987).

[25]P. G. de Gennes, Solid State Commun. **10**, 753 (1972); Mol. Cryst. Liq. Cryst. **21**, 49 (1973).

[26]J. Thoen, H. Beringhs, J. M. Auguste, and G. Sigaud, Liq. Cryst. **2**, 853 (1987).